PROBABILITY DISTRIBUTIONS OF CONCENTRATION FLUCTUATIONS OF A WEAKLY DIFFUSIVE PASSIVE PLUME IN A TURBULENT BOUNDARY LAYER

EUGENE YEE

Defence Research Establishment Suffield, Box 4000, Medicine Hat, Alberta, T1A 8K6 Canada

and

D. J. WILSON and B. W. ZELT

Department of Mechanical Engineering, University of Alberta, Edmonton, Alberta, T6G 2G8 Canada

(Received in final form 27 July, 1992)

Abstract. Results are presented from an experimental investigation of turbulent dispersion of a saline plume of large Schmidt number (Sc = 830) in a turbulent boundary-layer shear flow simulated in a laboratory water channel. The dispersion measurements are obtained in a neutrally buoyant plume from an elevated point source over a range of downstream distances where both plume meandering and fine-structure variations in the instantaneous plume are important. High-resolution measurements of the scalar fluctuations in the plume are made with a rake of conductivity probes from which probability distributions of concentration at various points throughout the plume are extracted from the time series.

Seven candidate probability distributions were tested, namely, the exponential, lognormal, clipped normal, gamma, Weibull, conjugate beta, and K-distributions. Using the measured values of the conditional mean concentration, $\underline{\chi}_p$, and the conditional fluctuation intensity, i_p, the Weibull distribution provided the best match to the skewness and kurtosis over all downstream fetches. The skewness and kurtosis were always overpredicted by the lognormal probability density function (pdf), and underpredicted by the gamma pdf. The conjugate beta distribution for which the model parameters are determined using a method of moments based on the fluctuation intensity, i_p, and skewness, S_p, was capable of modeling the distribution of scalar concentration over a wide range of positions in the plume.

1. Introduction

The statistical properties of scalar quantities, such as concentration and temperature, that are convected and mixed by a turbulent velocity field have practical importance in a diverse range of technological applications that span a wide variety of fields. For example, in the hazard assessment of toxic gas releases, it is important to consider short-term concentrations of the material occurring on time scales of seconds or minutes to account for the nonlinear relationship between concentration and toxic load, see Wilson (1991). Similar consideration apply to the assessment of nuisance due to malodourous materials and to the flammability of reactant substances, both of which require knowledge of the frequency at which contaminant concentrations exceed critical threshold values (e.g., lower flammability limit). Still further examples include air quality monitoring and regulation, the probability of visibility through a smoke screen, the effect of temperature fluctu-

Boundary-Layer Meteorology **64**: 321–354, 1993.

ations on the propagation of acoustic and electromagnetic waves, turbulent combustion where fast chemistry is determined by transport and small-scale mixing, and the design of efficient mixing and combustion devices.

Theoretical investigations, directed to the prediction of total moments of scalar fluctuations, have been based on a number of different approaches, e.g., Eulerian approaches based on a gradient-transfer approximation (Csanady, 1973), on a second-order closure of the diffusion equation (Sykes *et al.*, 1984), on large-eddy simulations in which unresolved or subgrid scales are modeled statistically using two-point closure theories (Antonopoulos-Domis, 1981), on semi-empirical Gaussian models predicated on a source-sink image hypothesis (Wilson *et al.*, 1985); Lagrangian approaches based on adoption of various stochastic models of fluid particle motion predicated on statistical scaling laws of turbulence (Durbin, 1980; Sawford, 1985; Kaplan and Dinar, 1988; Thomson, 1990); and on an approach based on similarity and dimensional arguments (Chatwin and Sullivan, 1979).

Since all these modeling approaches depend, in one form or another, on speculative or semi-empirical closure hypotheses, they require experimental measurements for the determination of their empirical parameters and for testing and validation of the closure hypotheses. In consequence, a number of full-scale atmospheric measurements of scalar fluctuations have been undertaken (Jones 1983; Hanna, 1984; Sawford *et al.*, 1985; Lewellen and Sykes, 1986; Sawford, 1987; Dinar *et al.*, 1988; Hanna and Insley, 1989; Mylne and Mason, 1991). Also, a number of laboratory measurements of concentration fluctuations have been made in wind tunnels, e.g., Warhaft (1984) and Stapountzis *et al.* (1986), who studied line-source heat dispersion in decaying grid turbulence and Fackrell and Robins (1982), who investigated point source dispersion of dilute hydrocarbon tracer from both surface and elevated sources in a turbulent, neutrally stable wind tunnel boundary layer. Deardorff and Willis (1984) have studied concentration fluctuations in buoyant and non-buoyant plumes (water-alcohol mixture with a small amount of Rhodamine-6G dye) under convective conditions in a water tank heated from below.

In the present experiments, the availability of a rake of fast-response concentration sensors enabled a number of concentration fluctuation statistics at various points in the dispersing plume to be determined. The behavior and modelling of the scalar concentration probability distribution at various points throughout the plume constitute the primary focus of the present study. Here, we are not concerned with the spatial distribution of the plume fluctuation statistics. For a description of the behavior of the cross-stream and vertical profiles of intermittency factor and various normalized central moments for the dispersing plume, the reader is referred to Wilson *et al.* (1991) and Bara *et al.* (1992). Our main objective here is to test several probability distribution functions for their accuracy in estimating skewness, kurtosis, and extreme values of plume concentration fluctuations. The data set used was measured as concentration time series by conductivity probes in a salt water plume from an elevated point source in a water channel boundary

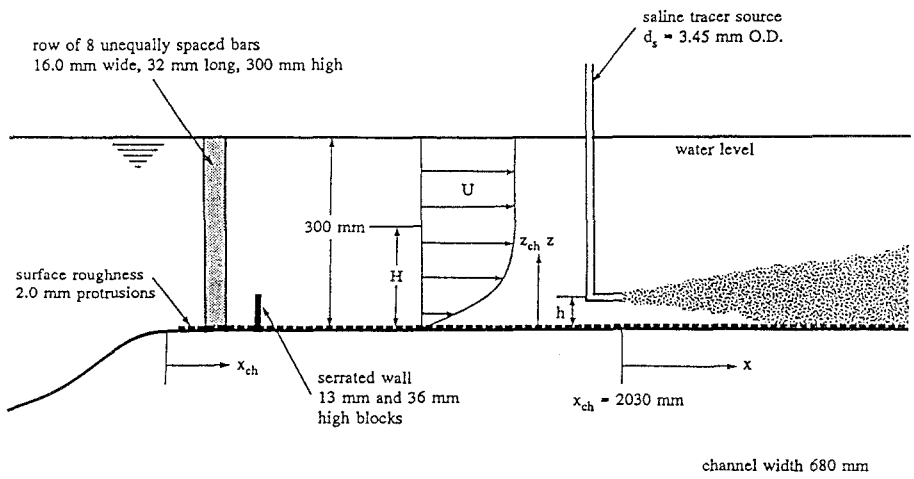

Fig. 1. Water channel configuration for dispersion in a rough surface boundary layer.

layer over a rough wall, as shown in Figure 1. This laboratory simulation of atmospheric dispersion in a neutrally stable boundary layer was able to generate stationary turbulence needed to produce long time series required for accurately estimating third and fourth moments in the intermittent fringes of the plume. The price of obtaining this stationary turbulence is the loss of large-scale cross-stream motions in the laboratory simulation. Because cross-stream turbulence and plume meandering is constrained by the water channel side walls, the laboratory simulation is limited to simulating atmospheric sampling times less than a few minutes. Although these laboratory simulations do not properly represent the large eddy structures and unsteady wind direction present in typical atmospheric measurements, they do nevertheless, provide a means for simulation of the idealized case of a steady wind direction.

Because the experiments involve the release of a saline tracer in water, the Schmidt number, Sc, of the scalar is much greater than unity (Sc $\approx$ 830 for the mixing of salt in water), so molecular diffusion effects are small, allowing concentration scales much smaller than the Kolmogorov microscale of velocity. The boundaries between unmixed material and mixed fluid are more sharply defined in the saline plumes as compared to those involving gaseous mixing in the atmosphere, for which Sc is of order unity.

2. Experimental Details

The concentration fluctuation measurements were conducted in a rectangular cross-section recirculating water channel in the Mechanical Engineering Department at the University of Alberta, and is described in Bara *et al.* (1992), and

shown schematically in Figure 1. A neutrally stable rough-wall boundary layer was produced by using a row of rectangular bars and a notched wall at the channel inlet, $x = -1800$ mm upstream of the saline tracer source, to accelerate development over the surface roughness. The roughness elements were an array of in-line cylinders 1.9 mm in height, 4.5 mm in diameter spaced 8.0 mm between centers in both cross-stream and downstream directions. This roughness array was formed by sheets of Leggo baseplate (a construction toy for children).

In the present study, a water depth of 300 mm was used to produce a boundary-layer thickness of $H = 150$ mm. The saline tracer source was a 4.2 mm O.D. tube injecting a neutrally buoyant mixture of water, ethanol and 50 gl^{-1} of salt isokinetically at a source height $h = 52$ mm, as shown in Figure 1. The mean velocity U and turbulence components $\overline{u^2}$, $\overline{w^2}$ and $\overline{uw}$ were determined by post-processing profiles at 0° and ±45° to the x-z plane using a single component laser doppler velocimeter (LDV) with 500 s sampling time to match the sample time of the saline conductivity probes. The data rate for velocity ranged from about 100 to 300 samples per second and depended on the density of the titanium oxide seeding particles used to operate the LDV in backscatter mode.

The mean velocity, U, agreed closely with the log-law profile, with von Karman's constant $\kappa = 0.4$:

$$U = \frac{u_*}{\kappa} \ln\left(\frac{z - d}{z_0}\right), \tag{1}$$

with $u_* = 14.6$ mm s^{-1}, $d = 1.5$ mm and $z_0 = 0.15$ mm. The velocity U at source height $h = 52$ mm was maintained at 210 mm s^{-1} for all the experiments. The friction velocity u_* estimated by extrapolating vertical profiles of $\overline{uw}$ to the surface yielded $u_* \approx 13.7$ mm s^{-1}, in good agreement with the value of 14. 6 mm s^{-1} found by fitting the log-law of Equation (1) to the mean velocity.

At source height, the integral scale L_u of streamwise velocity fluctuations increased gradually from 50 mm at $x = 0$ (the source location) to 70 mm at $x = 1000$ mm, indicating that the outer half of the boundary layer was still developing. Turbulence spectra were smooth and showed a decade of $-5/3$ inertial subrange. The normalized streamwise root-mean-square velocity, $(\overline{u^2})^{1/2}/u_*$, was found to be 1.85 at $z/H \approx 0.05$. The water channel facility and the measurement of the mean and turbulence velocity profiles are described in more detail in Wilson *et al.* (1991).

Fluctuating concentration measurements in the saline plume were obtained with a rake of 8 fast-response electrical conductivity probes with a 20 mm separation between probe tips. The effective spatial resolution of the conductivity probes, measured by dropping the probes through a sharp salt-water interface, was about 1.0 mm. With a mean velocity of $U = 210$ mm s^{-1} at source height, this produced a -6 dB point on the frequency response of the conductivity probes at about 30 Hz. Deconvolution of the digitized signals from the conductivity probes using

the inverse of the first-order impulse response function of the probes, produced an effective frequency response of about 90 Hz (−6 dB point). After deconvolution, the concentration sensor signal had an effective spatial resolution of about 0.3 mm.

The relative spatial resolution of the concentration fluctuation measurements can be assessed by comparing their effective spatial resolution with the smallest scales at which gradients can occur in both the velocity and concentration fields. The estimated value of the Kolmogorov microscale of velocity, $L_K \equiv (\nu^3/\bar{\epsilon})^{1/4}$, where ν is the kinematic viscosity of the fluid and $\bar{\epsilon}$ is the mean viscous dissipation rate, was about 0.35 mm ($\approx 2 \times 10^{-3}$ H) at the source height h. Because viscous dissipation occurs at length scales up to about $10L_K$, the effective spatial resolution of the concentration probes is sufficient to resolve scales at which viscous dissipation in the flow are important. However, for weakly diffusive scalars such as salt in water with Schmidt number, $\mathrm{Sc} \equiv \nu/D \approx 830$ (D is the molecular diffusivity of the scalar), the conduction cutoff scale (i.e., Batchelor length) at which molecular diffusion becomes important, $L_B \equiv (D^2\nu/\bar{\epsilon})^{1/4}$, is about 30 times smaller than L_K under the same conditions. In consequence, the conductivity probes used in this study were not able to resolve the concentration eddies at the smallest local scales at which gradients in the scalar field can be maintained by the flow. Zelt *et al.* (1987) showed that the loss of these small concentration eddies reduces the fluctuation variance by less than 5% for our water channel plumes.

3. Data Description and Preprocessing

Details of the water channel experiments, from which the data sets for the present study have been extracted, have been described by Wilson *et al.* (1991). The basic data consist of a set of concentration fluctuation time series of the saline tracer. Each time series was digitized with a 16-bit A/D converter on a LSI 11/23 computer at a digitizing frequency of 250 Hz for a time period of 500 s, to sample completely the spectrum of boundary-layer turbulence. It is important to note that, for the experiments, a sampling period of 500 s corresponded roughly to the passage of about 2000 integral length scales of turbulence over the receptor points and, consequently, provided a long enough sampling time for the accurate determination of concentration peaks caused by large-scale slow meandering. Instantaneous concentrations in the dispersing scalar spanned more than three decades in magnitude, requiring a digital resolution of 16 bits to accurately define the pdf of peak values. Concentration time series at 16 to 64 points in the lateral and vertical cross-sections of the plume were measured at three downstream distances from the source, at $x = 470$, 970, and 1500 mm (or, equivalently, at $x/h = 9.03$, 18.7, and 28.9).

Prior to performing the data analysis, some preprocessing of the concentration fluctuation time series was necessary, see Wilson *et al.* (1991). Firstly, small baseline drifts in the time series, due to the buildup of background salt concentra-

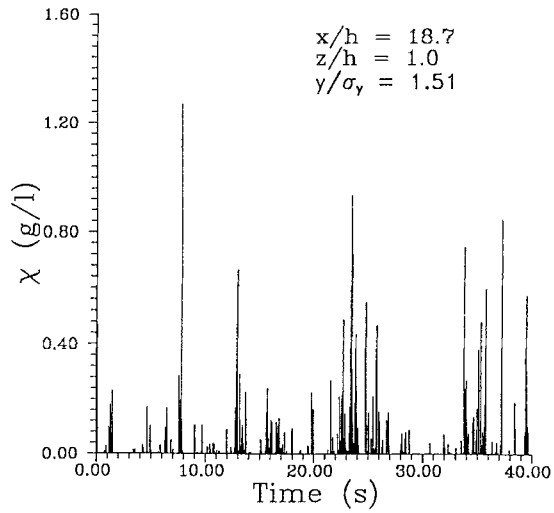

Fig. 2. A segment of the saline tracer concentration time series where both plume meandering and in-plume fine-scale turbulent mixing are important.

tion in the water channel and to electronic drift in the sensor output, were removed. Then deconvolution of the concentration time series was performed to correct for the instrumental smoothing, as described earlier. Finally, all values of the data sequences below a pre-determined threshold value were clipped to zero. The selection of the threshold value was determined from an analysis of the background concentration time series, obtained before and after each dispersion experiment, with the saline tracer source turned off. In this study, a threshold value of 8 standard deviations of the background noise level was used to define the zero concentration level for the determination of the intermittency, γ. The latter threshold was the minimum value required to produce a zero-period intermittency (i.e., $\gamma = 0$) in the background flow (viz., with the source turned off). The intermittency, γ, and total fluctuation intensity, i, are moderately sensitive to the choice of the threshold, with an uncertainty of ± 0.01 in the determination of the intermittency. The conditional fluctuation intensity, i_p, determined by ignoring zeros in the concentration time series, is much less sensitive to changes in threshold than are γ and i.

An example of a processed time trace of the saline tracer concentration in the plume is given in Figure 2, which displays 40 s (i.e., 10^4 data points) of saline concentration data obtained from a conductive probe positioned at source height $z/h = 1.0$ for a downstream distance $x/h = 18.7$ and a cross-stream position $y/\sigma_y = 1.51$. Here, y is the distance from the mean-plume centerline and σ_y is the cross-stream mean-plume dispersion, respectively. Figure 2 is very similar to concentration time series obtained from full-scale atmospheric measurements under near neutral stability conditions; see Jones (1983) and Mylne and Mason (1991). The

fluctuations in the dispersing plume occur on a wide range of time scales and, in particular, the plume reveals a highly intermittent structure in which the concentration variability is composed of a series of bursts of high concentration interspersed with periods of zero concentration. The concentration time series in Figure 2 shows two distinctly different mechanisms that produce fluctuations, namely, plume meandering in which turbulent eddies larger than the plume move it bodily back and forth over the receptor point to produce the intervals of zero concentration and turbulence on smaller scales than the plume width to produce rapid in-plume fluctuations.

4. Results

4.1. Observed probability distributions

The one-point probability density function (pdf) of concentration defines the distribution of scalar values found at a fixed point in the plume and, in consequence, provides statistical information on the frequency of concentration above critical threshold values. The probability distribution of scalar concentration embodies information on the time-independent advection and mixing processes in the plume.

The total probability density function of concentration must necessarily include the intervals of zero concentration characterized by the intermittency factor, γ, defined as the fraction of the total time that non-zero concentrations are observed. Conditional sampling of the concentration data to remove all intervals of zero concentration produce time traces from which the conditional (i.e., in-plume) concentration statistics can be obtained. After the removal of the intervals of zero concentration from the concentration time trace (viz., after conditional sampling), the exceedance probability distribution of the instantaneous concentration, χ, nondimensionalized by the local (conditional) mean concentration, $\overline{\chi_p}$, was compiled by sorting the data and determining the fraction of data points that exceeded prespecified multiples of $\chi/\overline{\chi_p}$.

Figure 3 presents measured exceedance probability distributions on the plume centerline for three downstream distances, $x/h = 9.03$, 18.7, and 28.9 at source height $z/h = 1.0$. Similarly, Figure 4 displays the exceedance probability distributions at the downstream distance $x/h = 28.9$ for various positions through the cross-stream plume cross-section. Note that, in terms of the normalized concentration variable, the probability distributions collapse remarkably well to a nearly self-similar form, especially at various positions through the cross-section at a fixed downstream distance. These results suggest that $\chi/\overline{\chi_p}$ is a proper similarity variable for in-plume concentration fluctuations, and that the various higher-order moments of the probability distribution of $\chi/\overline{\chi_p}$ are largely independent of lateral position in the plume. Note that the tails of the observed concentration probability distributions are rather elongated and peak concentrations greater than 10 times the

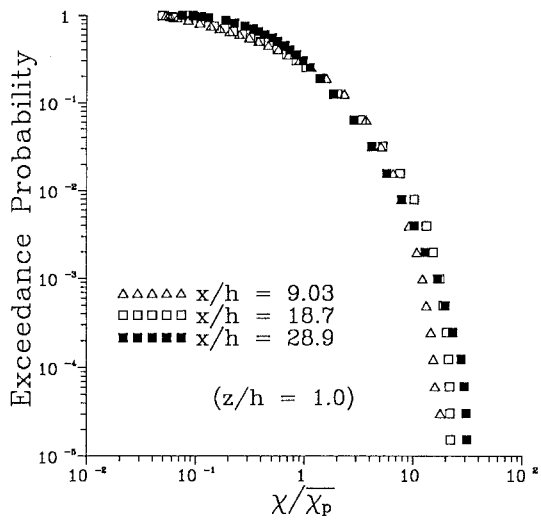

Fig. 3. Exceedance probability distributions of the conditionally sampled and normalized concentrations, $\chi/\overline{\chi_p}$, measured at source height on the mean-plume centerline at three downstream locations.

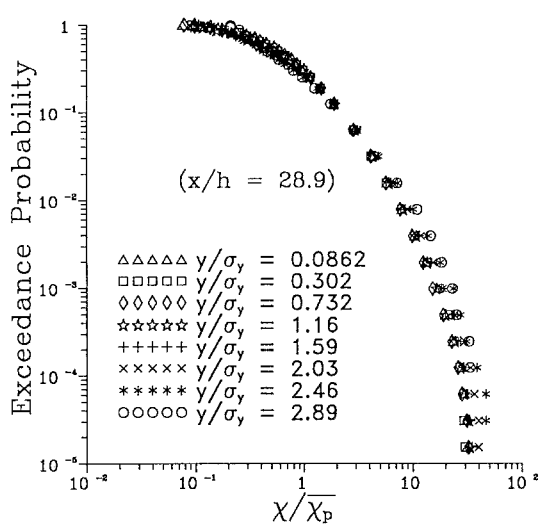

Fig. 4. Exceedance probability distributions of the conditionally sampled and normalized concentrations, $\chi/\overline{\chi_p}$, measured at source height at the normalized downstream distance $x/h = 28.9$ for various points in the cross-stream cross-section of the plume.

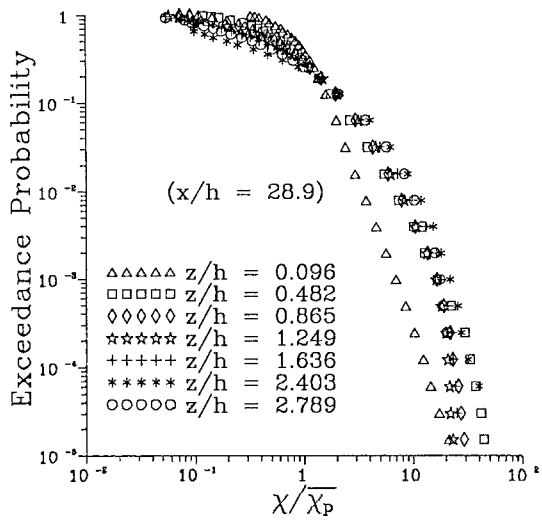

Fig. 5. Exceedance probability distributions of the conditionally sampled and normalized concentrations, $\chi/\overline{\chi_p}$, measured on the mean-plume centerline at the normalized downstream distance $x/h = 28.9$ for various points in the vertical cross-section of the plume.

conditional mean concentration are observed with a probability of ≈0.01. The probability distributions of normalized concentration are strongly non-Gaussian with a long tail caused by high concentrations in localized unmixed patches.

Figure 5 shows measurements of the exceedance probability distribution obtained at several points through a vertical cross-section of the plume at $x/h = 28.9$. In this case, self-similarity of the distributions is not observed because pdfs near the ground are markedly different than those obtained at source height. In particular, the distributions measured near the surface exhibits shorter lower and upper tails (viz., the distributions are less elongated in both tails) than those measured farther above the ground, implying that both very low and very high concentrations are observed with smaller frequency near the ground. The shorter tails found in the probability distributions of concentration near the ground surface are a consequence of increased wind shear, and decreased integral scale near $z = 0$ that smear out the small-scale inhomogeneities within the plume. The effect of shear is to increase mixing and the rate of decay of scalar fluctuations, and this effect is most prevalent very near the ground where the mean shear is greatest. In Figure 5, only the probability distribution measured at $z/h = 0.096$ is significantly altered by surface effects. At $z/h = 0.096$, the mean shear $\tau \equiv \mathrm{d}U/\mathrm{d}z = u_*/(\kappa(z - \mathrm{d}))$ is about $10.5\ \mathrm{s}^{-1}$ (cf. Equation (1)), and we observe that the probability distribution measured at this position has a noticeably shorter upper tail than those measured at greater heights. However, the effect of shear diminishes rapidly with distance from the surface so that even at $z/h = 0.482$, the mean shear, τ, has decreased to

about $1.5\,s^{-1}$ and the probability distribution measured here resembles those measured at greater distances above the surface.

4.2. Modeled probability distributions

The conserved scalar cumulative distribution function (cdf), $F_T(\chi)$, at any point in the plume is composed of a mixed fluid part, denoted by $F(\chi)$, that results from in-plume mixing of eddies that contain the scalar contaminant, and an unmixed ambient fluid part, denoted by $F^-(\chi)$, that is caused by plume meandering producing intermittent periods of zero concentration for a fraction of time $(1-\gamma)$. In consequence, the cdf of the total concentration can be written as

$$\begin{aligned} F_T(\chi) &= \gamma F(\chi) + (1-\gamma)F^-(\chi) \\ &= \gamma F(\chi) + (1-\gamma)H(\chi)\,. \end{aligned} \tag{2}$$

Since there is a finite probability, $(1-\gamma)$, of observing periods of zero concentration, the probability distribution $F^-(\chi)$ in Equation (2) is expressed as a unit step function, $H(\chi)$, with a step at $\chi = 0$ of magnitude $(1-\gamma)$. Differentiating Equation (2), the pdf of scalar concentration is

$$p_T(\chi) \equiv \frac{dF_T(\chi)}{d\chi} = \gamma p(\chi) + (1-\gamma)\,\delta(\chi)\,, \tag{3}$$

where $p_T(\chi)$ is the total pdf of concentration, $p(\chi)$ is the pdf for in-plume fluctuations, and $\delta(\chi)$ is a Dirac delta function which arises from the step discontinuity. According to Equation (3), once the intermittency factor, γ, is known, the pdf of the total concentration, $p_T(\chi)$, is completely determined by $p(\chi)$, the conditional pdf for the concentration fluctuations with the intervals of zero concentration removed.

The present study tested seven functional forms for the conditional pdf of scalar concentration. The seven chosen were the lognormal distribution (Csanady, 1973), the exponential distribution (Hanna, 1984), the clipped normal distribution (Lewellen and Sykes, 1986), the gamma distribution (Wilson and Simms, 1985), the Weibull distribution, the conjugate beta distribution, and the K-distribution. The functional form and the first four moments of each of these model distributions are summarized in Appendix A. All the candidate distributions are standard, except for the conjugate beta distribution (which will be dealt with in greater detail later in this paper) and the K-distribution. A K-distributed random variable is obtained from a Rayleigh-distributed random variable with a mean value distributed according to a chi-square distribution; the shape parameter, ν, for the K-distribution (cf. Appendix A) provides a measure of the "spikiness" of the random process. For a given variance of a K-distributed random variable, the pdf has a longer tail for smaller values of the parameter, ν (i.e., smaller values of ν are associated with longer-tailed, more spiky (intermittent) processes). It can be

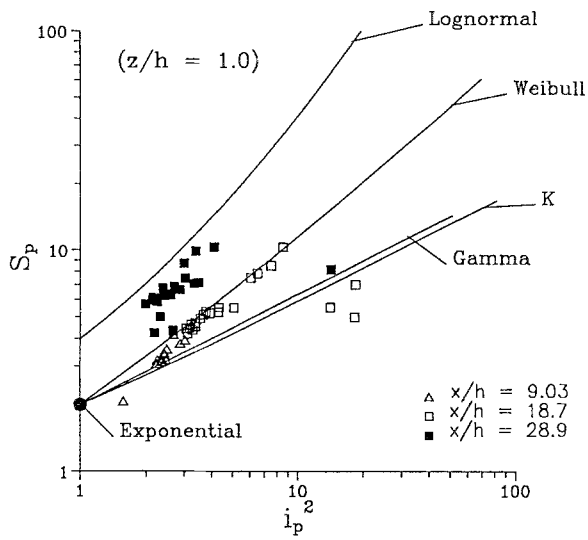

Fig. 6. Concentration data, measured at source height for various points in the cross-stream plume cross-section at three downstream locations, plotted on a (i_p^2, S_p) diagram (viz., fluctuation intensity and skewness space). The plot also includes the theoretical one-dimensional curves generated by five model distributions. The exponential distribution is represented by a single point in the (i_p^2, S_p) diagram.

shown that all the moments of the K-distribution lie between those of a Rayleigh and a lognormal distribution having the same mean and variance.

In order to determine which of the model probability distributions best represents the concentration fluctuation data, the normalized moments (e.g., fluctuation intensity, skewness, and kurtosis) of the conditional data are compared with the corresponding moments predicted by the candidate distributions. In this regard, we concentrate exclusively on the three normalized moments of greatest interest; the relative fluctuation intensity, $i_p^2 \equiv \sigma_{\chi,p}^2/\chi_p^2$, the skewness, $S_p \equiv \overline{(\chi - \bar{\chi}_p)^3}/\sigma_{\chi,p}^3$, and the kurtosis, $K_p \equiv \overline{(\chi - \bar{\chi}_p)^4}/\sigma_{\chi,p}^4$. Here, the subscript p is used to denote the conditional statistic and $\sigma_{\chi,p}^2 = \overline{(\chi - \bar{\chi}_p)^2}$ is the conditional variance of the scalar fluctuations. To identify an appropriate probability distribution model for the conditional concentration data from a number of candidate models, we compare the relationship between S_p or K_p and i_p^2 for the observed data and the corresponding prediction produced by the various model distributions. The method of moments, based on the conditional mean concentration and conditional fluctuation intensity, was used to obtain estimates for the model parameters that characterize the exponential, lognormal, gamma, Weibull, conjugate beta, and K-distributions.

Figure 6 presents a comparison of the $S_p - i_p^2$ relationship, obtained from concentration data at source height for various cross-stream positions in the plume and at various downstream distances from the source, with the candidate model distributions. Similarly, Figure 7 displays a comparison of the $K_p - i_p^2$ relationship for data and model predictions. The prediction provided by the clipped normal

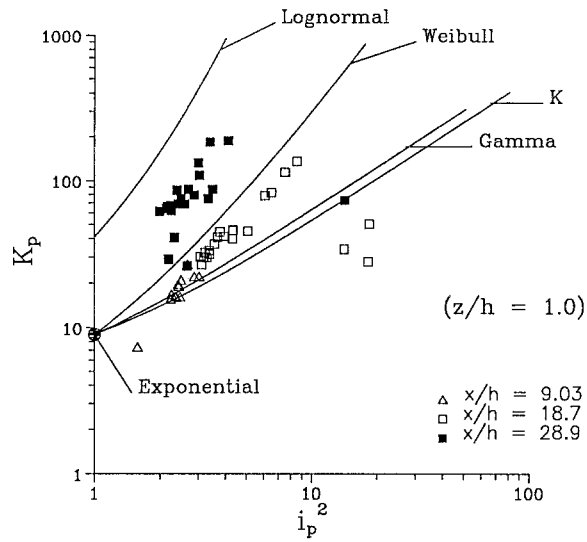

Fig. 7. Concentration data, measured at source height for various points in the cross-stream plume cross-section at three downstream locations, plotted on a (i_p^2, K_p) diagram (viz., fluctuation intensity and kurtosis space). The plot also includes the theoretical one-dimensional curves generated by five model distributions. The exponential distribution is represented by a single point in the (i_p^2, K_p) diagram.

distribution has not been included in Figures 6 and 7 because this distribution requires $i_p^2 \leq 1$ (cf. Appendix B), whereas all the data points show $i_p^2 > 1$. Consequently, the clipped normal distribution was eliminated as an appropriate model for these concentration data. Finally, Figures 8 and 9 present the same comparisons as Figures 6 and 7, respectively, but with the concentration data obtained at different heights and downstream locations on the plume centerline. The clipped normal curve has been included in Figures 8 and 9 because we observed 4 data points with $i_p^2 < 1$. However, even for these data points, we note that the clipped normal distribution greatly underestimates both the skewness, S_p, and kurtosis, K_p, of the measured concentration data. Again, we can eliminate the clipped normal distribution as an appropriate model for our concentration data.

Except for the exponential distribution, which maps into a point in the (i_p^2, S_p) and (i_p^2, K_p) diagrams, all the exhibited candidate distributions fall on one-dimensional curves on the diagrams. In consequence, the probability model that best characterizes the distribution of concentration data is the one whose curve in the (i_p^2, S_p) and (i_p^2, K_p) planes lies closest to the data points. On Figures 6 to 9, the majority of the data points in the (i_p^2, S_p) and (i_p^2, K_p) planes are bounded above and below by the lognormal and gamma distributions, respectively. Because the characteristics of a probability distribution in the upper tail are most evident in its higher-order moments such as skewness and kurtosis, this observation implies that the lognormal and gamma distributions possess longer and shorter tails,

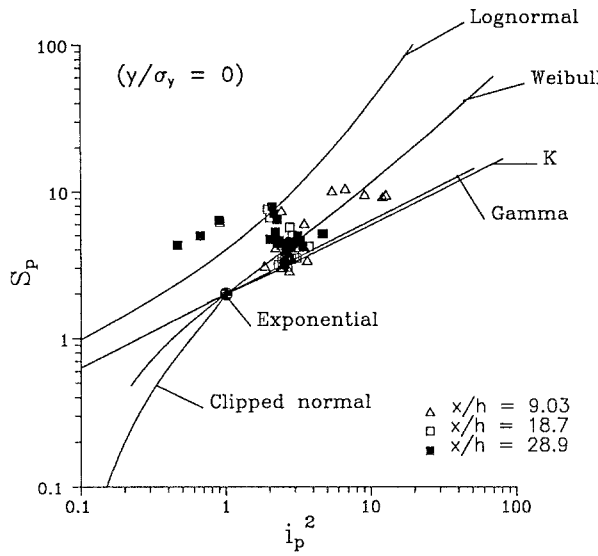

Fig. 8. Concentration data, measured on the mean-plume centerline for various points in the vertical plume cross-section at three downstream locations, plotted on a (i_p^2, S_p) diagram (viz., fluctuation intensity and skewness space). The plot also includes the theoretical one-dimensional curves generated by six model distributions. The exponential distribution is represented by a single point in the (i_p^2, S_p) diagram.

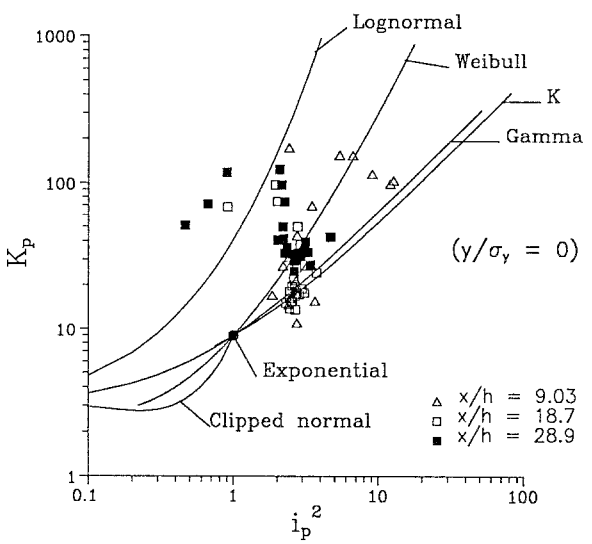

Fig. 9. Concentration data, measured on the mean-plume centerline for various points in the vertical plume cross-section at three downstream locations, plotted on a (i_p^2, K_p) diagram (viz., fluctuation intensity and kurtosis space). The plot also includes the theoretical one-dimensional curves generated by six model distributions. The exponential distribution is represented by a single point in the (i_p^2, K_p) diagram.

respectively, than the concentration data. On these moment diagrams, it is noted that the Weibull distribution provides the best match to the data close to the source. However, at $x/h = 28.9$, the lognormal distribution is seen to provide a better approximation to the observed data although most of the data still fall below the lognormal curve. At $x/h = 9.03$, the gamma distribution provides a good approximation. In general, most of the data points plotted on the (i_p^2, S_p) and (i_p^2, K_p) diagrams of Figures 6 to 9 do not lie near any of the curves generated by the candidate model distributions. A more quantitative comparison between the data and model distributions will be made presently with reference to the observed and predicted moments and concentration quantiles.

To assess the goodness-of-fit of these distributions as a model for the total statistical distribution of scalar concentration including zero concentration intervals, we compared data and model predictions of the total skewness, S, and the total kurtosis, K. It follows directly from their definitions that the total normalized moments are related to the conditional normalized moments and the intermittency factor as follows:

$$i^2 = \frac{i_p^2 + 1}{\gamma} - 1 , \tag{4}$$

$$S = \frac{1}{\gamma^{1/2}[1 + (1 - \gamma)/i_p^2]^{3/2}} \left\{ S_p + \frac{3(1 - \gamma)}{i_p} + \frac{(2\gamma - 1)(\gamma - 1)}{i_p^3} \right\} , \tag{5}$$

and

$$K = \frac{1}{\gamma[1 + (1 - \gamma)/i_p^2]^2} \times \left\{ K_p + \frac{4(1 - \gamma)S_p}{i_p} + \frac{6(1 - \gamma)^2}{i_p^2} + \frac{(1 - \gamma)(1 - 3\gamma + 3\gamma^2)}{i_p^4} \right\} . \tag{6}$$

Figures 10 to 13 display the observed total skewness and kurtosis against the model distribution predictions for these normalized moments for the lognormal, gamma, Weibull, and conjugate beta distributions, respectively. The solid line in these figures indicates the locus of points that correspond to perfect agreement between the observed and predicted normalized moments. The behavior of the lognormal and gamma distributions exhibited in Figures 10 and 11 are consistent with the results presented for the conditional moments in Figures 6 to 9. The lognormal distribution (Figure 10) provides an upper bound to the data in the sense that its predicted third and fourth moments approximately delineate the maximum in the observed third and fourth moments for various positions in the dispersing plume. The overprediction of these moments by the lognormal distribution is less severe at the greater downstream distances at which the internal patchiness within the plume is more important than meandering in generating concentration fluctuations. Conversely, the gamma distribution (Figure 11) defines

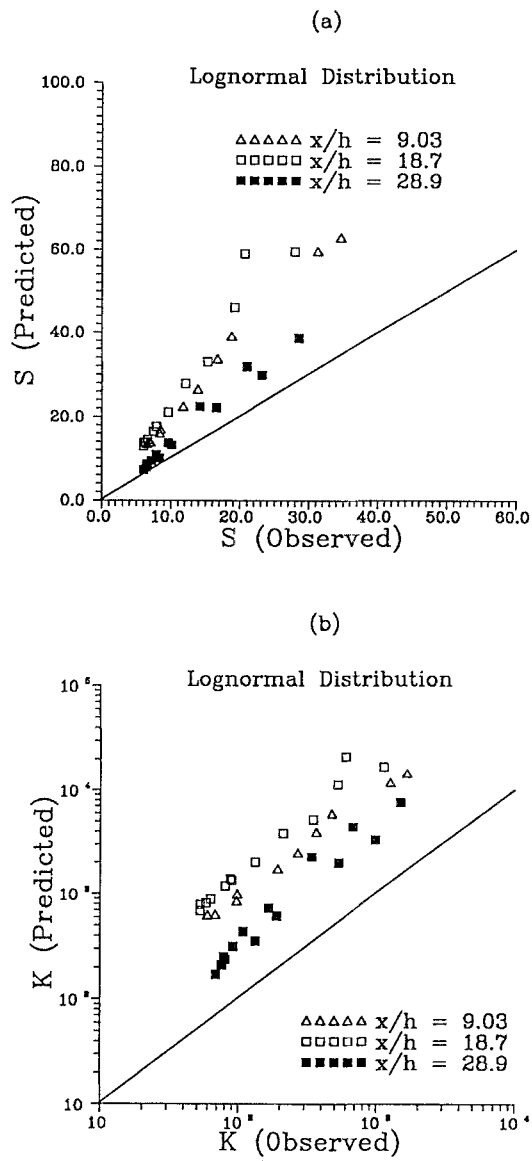

Fig. 10. Scatterplot of (a) the observed total skewness versus the predicted total skewness and (b) the observed total kurtosis versus the predicted total kurtosis for the lognormal distribution. The data points were obtained at source height for various points in the lateral cross-section of the continuous plume at three downstream locations.

a lower bound for the third and fourth moments. The gamma distribution provides good predictions over those downstream fetches where plume meandering constitutes the dominant contribution to the concentration fluctuations.

The Weibull distribution (Figure 12) provides a good overall prediction of the

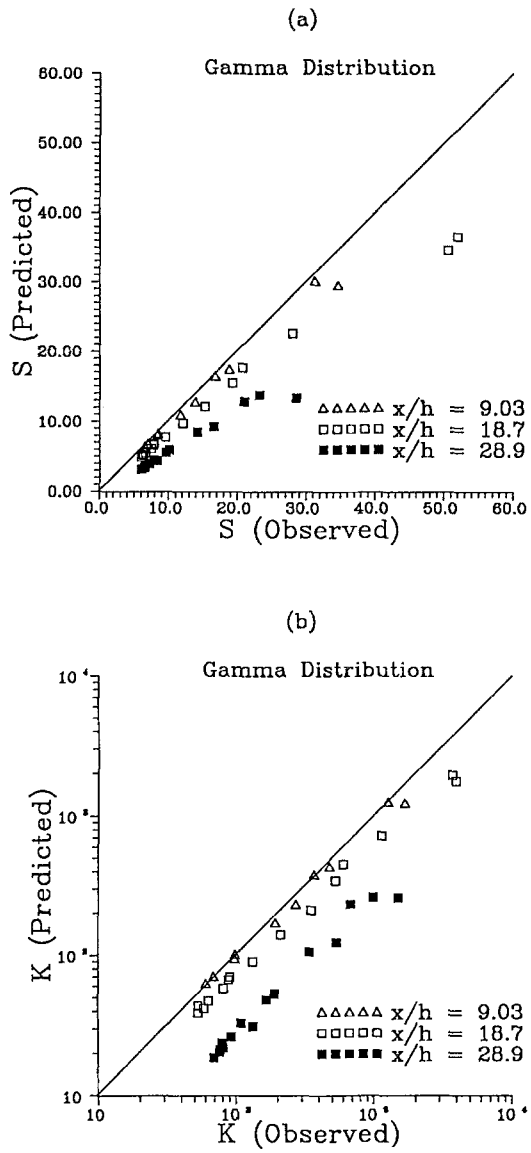

Fig. 11. Scatterplot of (a) the observed total skewness versus the predicted total skewness and (b) the observed total kurtosis versus the predicted total kurtosis for the gamma distribution. The data points were obtained at source height for various points in the cross-stream cross-section of the continuous plume at three downstream locations.

normalized total moments over a broad range of downstream fetches. In general terms, this distribution slightly overpredicts the normalized moments in the plume at downstream distances from the source where plume meander provides a significant contribution to the concentration fluctuations. At greater distances from the

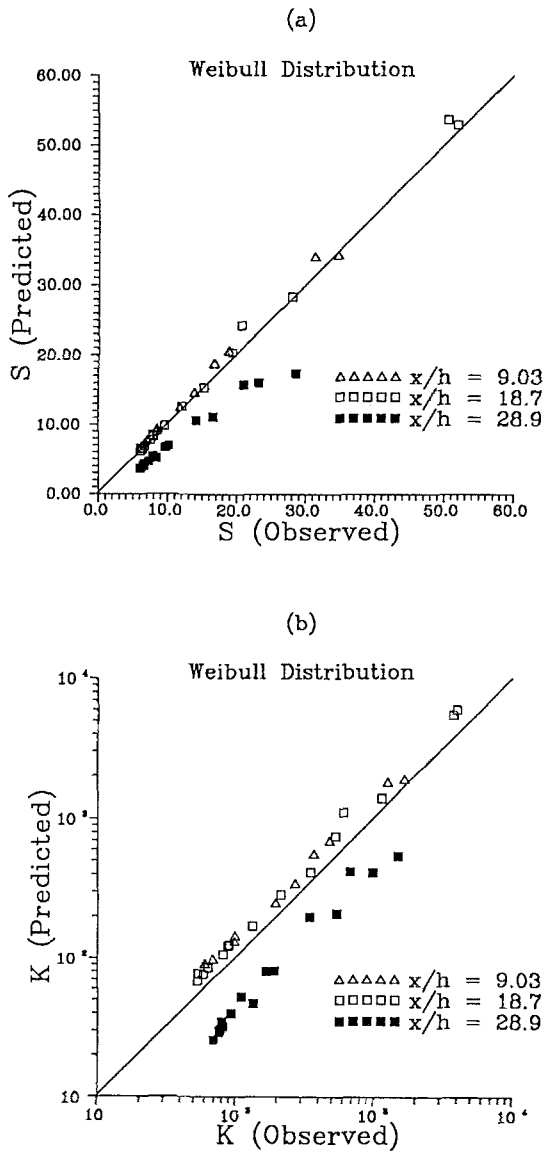

Fig. 12. Scatterplot of (a) the observed total skewness versus the predicted total skewness and (b) the observed total kurtosis versus the predicted total kurtosis for the Weibull distribution. The data points were obtained at source height for various points in the cross-stream cross-section of the continuous plume at three downstream locations.

source, where the developing internal structure of the plume becomes the dominant contribution to the concentration fluctuations, the Weibull distribution moderately underpredicts the total moments.

The conjugate beta distribution (Figure 13) provides good predictions for the

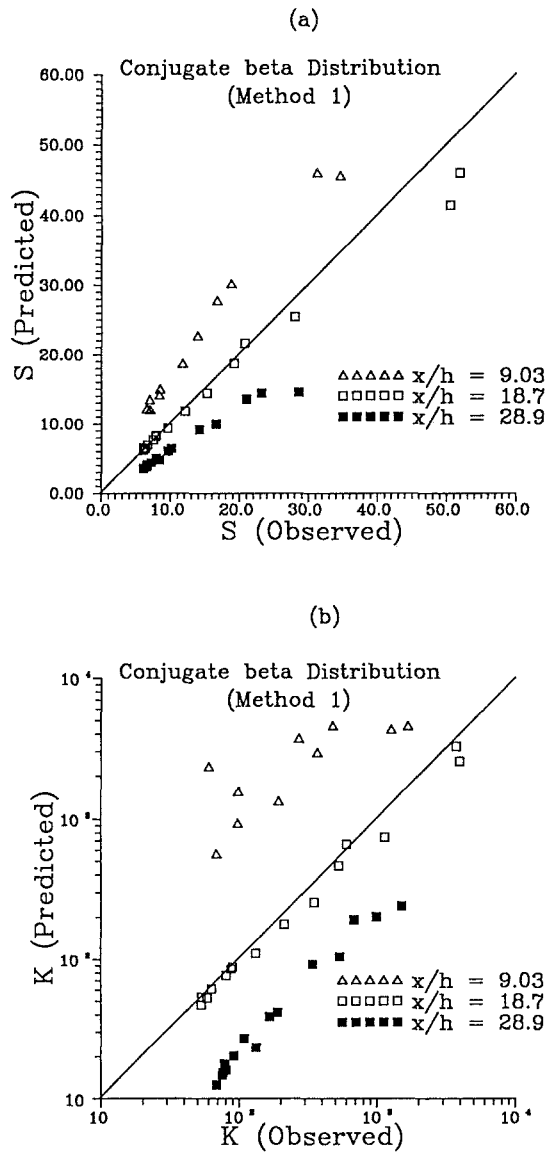

Fig. 13. Scatterplot of (a) the observed total skewness versus the predicted total skewness and (b) the observed total kurtosis versus the predicted total kurtosis for the conjugate beta distribution in which the parameters are estimated using the method of moments based on the conditional concentration and fluctuation intensity (Method 1). The data points were obtained at source height for various points in the cross-stream cross-section of the continuous plume at three downstream locations.

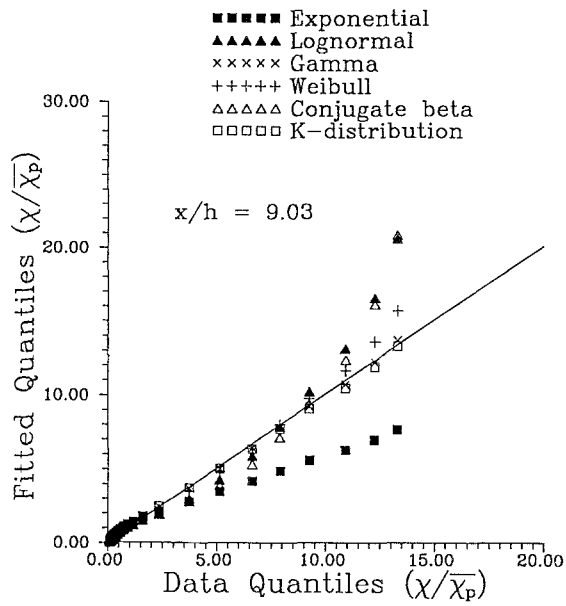

Fig. 14. The quantile-quantile (Q-Q) plot comparing the normalized concentration data quantiles with the associated model quantiles of six fitted probability distributions. The data was extracted from a point at source height on the mean-plume centerline at the downstream location $x/h = 9.03$. The model parameters for the fitted probability distributions were obtained using the method of moments based on the mean concentration, $\overline{\chi_p}$, and the fluctuation intensity, i_p^2.

total moments at those ranges where meandering and internal structure of the plume provide roughly comparable contributions to the concentration fluctuations. However, this distribution overpredicts the total moments at shorter downstream fetches corresponding to the meander-dominated stage of plume development and underpredicts the moments at longer fetches corresponding to the internal structure-dominated stage of plume development. In the next section, we shall show that the main advantage of the conjugate beta distribution is its flexibility in covering a region rather than a line in the (i_p^2, S_p) and (i_p^2, K_p) planes.

To see how well the model distributions represent the concentration data, Figures 14 to 16 display quantile-quantile (Q-Q) plots, with the quantiles of the normalized data (viz., $\chi/\bar{\chi}_p$) on the horizontal axis and those predicted by the fitted distributions on the vertical axis. The data used to construct Figures 14 to 16 were obtained at source height $z/h = 1.0$ along the mean-plume centerline $y/\sigma_y = 0$ from three downstream locations in the plume. Recall that if q denotes a proper positive fraction, then the quantile of order q (or, equivalently, the $100q$ percentile), which will be designated by χ_q, is defined by the unique solution of the equation $F(\chi_q) \equiv \Pr\{\chi \leq \chi_q\} = q$. In the Q-Q plots shown in Figures 14 to 16, the solid line denotes the locus of points that correspond to an exact (or, ideal) fit between the observed distribution and the model distribution and, in effect,

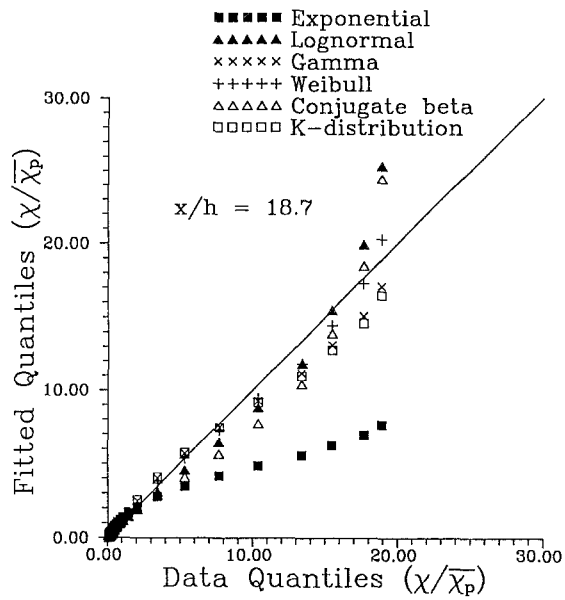

Fig. 15. The quantile-quantile (Q-Q) plot comparing the normalized concentration data quantiles with the associated model quantiles of six fitted probability distributions. The data were extracted from a point at source height on the mean-plume centerline at the downstream location $x/h = 18.7$. The model parameters for the fitted probability distributions were obtained using the method of moments based on the mean concentration, $\overline{\chi_p}$, and the fluctuation intensity, i_p^2.

corresponds to a straight line that has slope 1 and intercept 0 when the abscissa (data quantiles) and ordinate (fitted quantiles) have equal scales. The results of Figures 14 to 16 are consistent with those displayed in Figures 10 to 13. The gamma pdf (cf. Figure 14) provides the best representation of the data at the short downstream fetches corresponding to the meander-dominated stage of plume development. The Weibull pdf provides the best overall representation of the data over a wide range of downstream fetches from the meander-dominated to the internal-structure dominated stage of plume development. The quantiles of the lognormal pdf provide an upper bound to the data quantiles over the entire range of downstream positions.

5. Conjugate Beta Distribution

Figures 6 to 9 indicate that the normalized moments of the concentration data are distributed over a rather extended region of the (i_p^2, S_p) and (i_p^2, K_p) diagrams and, in consequence, cannot be modeled adequately by any probability distribution that generates only a one-dimensional curve on the diagrams (e.g., lognormal, gamma, Weibull distributions). The normalized moments for the concentration data lie primarily on or above the line $S_p = 2i_p$ in the (i_p^2, S_p) diagram, which

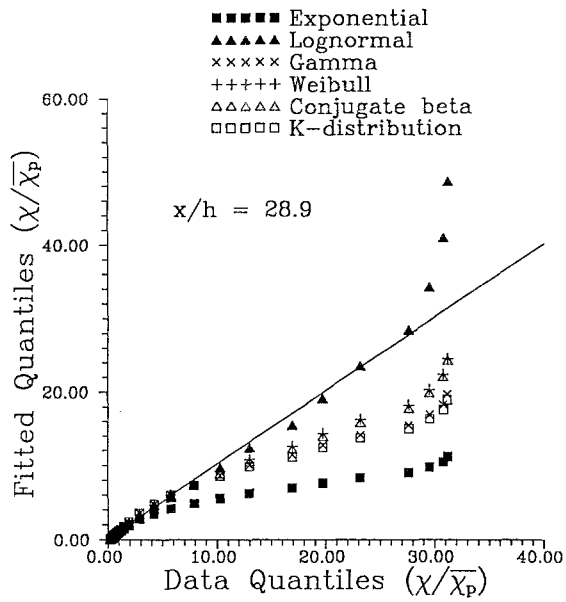

Fig. 16. The quantile-quantile (Q-Q) plot comparing the normalized concentration data quantiles with the associated model quantiles of six fitted probability distributions. The data was extracted from a point at source height on the mean-plume centerline at the downstream location $x/h = 28.9$. The model parameters for the fitted probability distributions were obtained using the method of moments based on the mean concentration, $\overline{\chi_p}$, and the fluctuation intensity, i_p^2.

corresponds to the curve mapped out by the gamma distribution. Consequently, to model the probability distribution of concentration at various positions in the dispersing plume, what is desired is a model distribution which maps into the upper region of the (i_p^2, S_p) plane that is bounded below by the line $S_p = 2i_p$. Such a model distribution would have the important advantage that it would be able to describe the probability distribution of concentration at various positions in the plume without any change in functional form.

One possible candidate for a distribution model that can cover a region of the (i_p^2, S_p) plane without having to change its functional form is the beta distribution,

$$p(\chi) = \frac{1}{B(\alpha, \beta)} \chi^{\alpha-1}(1-\chi)^{\beta-1}, \tag{7}$$

where $B(\alpha, \beta)$ denotes the beta function. The beta distribution has been proposed as a model for the pdf of contaminant concentrations by Effelsberg and Peters (1983) and by Chatwin and Sullivan (1987). Unfortunately, the beta distribution is not an appropriate model for our concentration data since the beta distribution covers the (i_p^2, S_p) plane below the line $S_p = 2i_p$, whereas the normalized moments of the concentration data lie mostly above this line. As an alternative, we propose the use of a pdf of the form

$$p(\chi) = \frac{1}{B(\alpha, \beta)} \frac{\chi^{\alpha-1}}{(1+\chi)^{\alpha+\beta}}, \tag{8}$$

which will be referred to as the conjugate beta distribution. The conjugate beta distribution was developed from a consideration of the alternative integral representation for the incomplete beta function (Spanier and Oldham, 1987):

$$B(\alpha, \beta; \chi/(1+\chi)) = \int_0^{\chi} \frac{t^{\alpha-1}}{(1+t)^{\alpha+\beta}} \, dt . \tag{9}$$

In contrast to the beta distribution, the conjugate beta distribution covers the appropriate upper region of the (i_p^2, S_p) plane above the line $S_p = 2i_p$. To justify this claim, the two shape parameters, α and β, that determine the conjugate beta distribution can be expressed explicitly in terms of the relative fluctuation intensity, i_p^2, and the skewness, S_p, as follows (cf. Appendix A):

$$\alpha = \frac{2(S_p i_p - i_p^2 + 1)}{4i_p^2 + S_p i_p (i_p^2 - 1)} \tag{10}$$

and

$$\beta = \frac{4i_p^2 - 3S_p i_p - 2}{2i_p^2 - S_p i_p} . \tag{11}$$

Equations (10) and (11) show that there is a one-to-one correspondence between the shape parameters, α and β, of the conjugate beta distribution and the normalized moments, i_p^2 and S_p, that define the points on the (i_p^2, S_p) plane. From the inverse of the mappings exhibited by Equations (10) and (11) (cf. Appendix A), it can be shown that the admissible values for α and β map the conjugate beta distribution into points in the (i_p^2, S_p) plane above the line $S_p = 2i_p$, which is the locus of points in the plane that determine the gamma distribution. Furthermore, it can be shown that the conjugate beta distribution asymptotically approaches the gamma distribution in the limit as $\beta \to \infty$, provided α remains finite. Since almost all the observed normalized moment pairs (i_p^2, S_p) lie on or above the line $S_p = 2i_p$, the conjugate beta distribution is an appropriate statistical model for the concentration data because it is capable of covering the relevant region of the (i_p^2, S_p) plane by changing only the parameters of the distribution while maintaining the same functional form.

Of the seven candidate model distributions considered, the conjugate beta distribution is the only one for which the higher-order normalized moments (e.g., fluctuation intensity, skewness, kurtosis, etc.) depend on both model parameters. In consequence, the conjugate beta distribution possesses a greater flexibility in allowing one to match higher-order moments of the data. Previously, we applied the method of moments by specifying the mean, $\overline{\chi_p}$, and fluctuation intensity, i_p, to determine the parameters α and β of the conjugate beta distribution. This

procedure implicitly forces one of the parameters of the conjugate beta distribution to function as a scale parameter and, in consequence, the conjugate beta distribution maps a line rather than a region in the (i_p^2, S_p) plane. Alternatively, we can set the parameters of the conjugate beta distribution to match the measured fluctuation intensity, i_p, and skewness, S_p, rather than $\overline{\chi_p}$ and i_p. This allows both parameters of the conjugate beta distribution to function as shape parameters to cover the admissible portion of the (i_p^2, S_p) plane. Specifying i_p and S_p differs from the conventional approach of selecting the mean concentration and the fluctuation intensity as the quantities that are used in the moment-matching algorithm for the determination of the model parameters (e.g., Wilson and Simms, 1985; Lewellen and Sykes, 1986; Sawford, 1987; Dinar *et al.*, 1988; Mylne and Mason, 1991). To compare the i_p, S_p method to specifying $\overline{\chi_p}$, i_p, Equations (10) and (11) were used to estimate α and β with i_p^2 and S_p determined from the concentration time trace. The moment-matching algorithm based on i_p^2 and S_p uses normalized quantities, and so has the added advantage that it does not require calibrated concentration data.

The goodness-of-fit of the conjugate beta distribution obtained from the method of moments based on i_p^2 and S_p was assessed by comparing data quantiles with model quantiles for the normalized concentration $\chi/\overline{\chi_p}$. For comparison with Figure 16, we chose a point in the continuous plume at $x/h = 28.9$ on the mean plume centerline at source height. Figure 17 exhibits the lognormal and conjugate beta Q-Q plots for normalized concentration. In this figure, the crosses are the conjugate beta predictions for the concentration data quantiles for a method of moments based on $\overline{\chi_p}$ and i_p^2, designated as Method 1; for comparison, the conjugate beta predictions of the data quantiles for a method of moments based on i_p^2 and S_p, referred to as Method 2, are indicated by the open triangles. In the central to mid-extreme range of the concentration data, the conjugate beta distribution determined using Method 2 and the lognormal predictions represent the data roughly equally well. However, in the extreme upper tail, the Q-Q plot of the conjugate beta distributions (Method 2) exhibits an upward convex curvature toward the vertical suggesting that the upper tail of the conjugate beta distribution is slightly heavier than observed. Although the conjugate beta distribution (Method 2) tends to overpredict the data quantiles in the extreme upper tail, this overprediction is not as severe as the lognormal distribution. Indeed, the conjugate beta distribution based on Method 2 overpredicts the 1×10^{-5} exceedance probability level of concentration by about 30% whereas the lognormal distribution overpredicts the same concentration level by about 60%.

The kurtosis can be used as another measure of tailweight of probability distribution. The lognormal distribution overpredicts the kurtosis, K_p, by about 200%; by comparison, the conjugate beta distribution for which the parameters are determined using Methods 1 and 2 underpredict and overpredict, respectively, K_p by about 85% and 40%. Figure 18 exhibits the conjugate beta prediction (Method 2) for the total kurtosis, K, where it is seen that the conjugate beta distribution

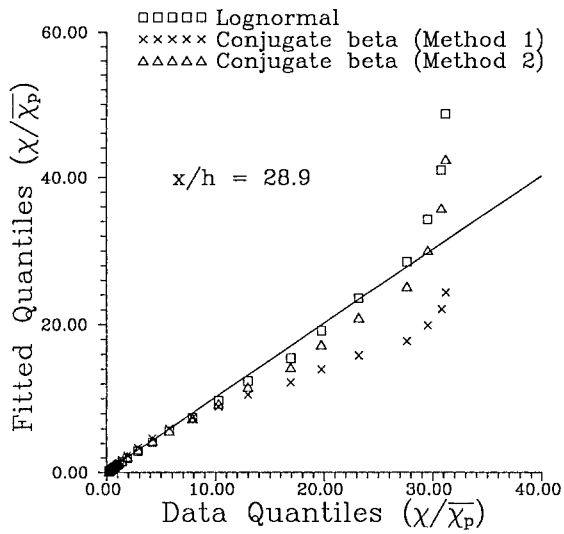

Fig. 17. The quantile-quantile (Q-Q) plot comparing the normalized concentration data quantiles with the associated model quantiles of the fitted lognormal and conjugate beta distributions. The data were extracted from a point at source height on the mean-plume centerline at the downstream location $x/h = 28.9$. The model parameters for the fitted conjugate beta distributions were determined using two different methods, namely, a method of moments based on the mean concentration, $\overline{\chi_p}$, and the fluctuation intensity, i_p^2 (Method 1) and a method of moments based on the fluctuation intensity, i_p^2, and the skewness, S_p (Method 2).

(Method 2) slightly overpredicts the kurtosis for points in the continuous plume at $x/h = 28.9$ in the internal structure-dominated regime of plume development. This implies that the upper tail of the model distribution is slightly elongated relative to the observed probability distribution of concentration. Along the same lines, it is noted that the conjugate beta distribution (Method 2) slightly underpredicts the kurtosis for points in the dispersing plume where plume meander constitutes a major contribution to concentration fluctuations. In summary, the conjugate beta distribution, with parameters α and β determined by i_p^2 and S_p, provides a better match to the concentration data, viz., the model only slightly overestimates or underestimates the frequency of high concentrations, overpredicting or underpredicting the 1×10^{-5} exceedance level of concentration by less than 50%.

The conjugate beta distribution provides an adequate and versatile model for the distribution function of our normalized concentration data, since it can be made to cover an admissible portion of the (i_p^2, S_p) plane. The price of obtaining this modeling versatility is the need to use the skewness, S_p, for the determination of the distribution parameters. For the purpose of model parameterization, this would require the prediction of three parameters in addition to the mean concentration, $\bar{\chi}$ (or, equivalently, $\overline{\chi_p}$), in order to fully specify the total pdf of concentration, namely, γ, i^2, and S (or, equivalently, i_p^2 and S_p). The procedure (Method

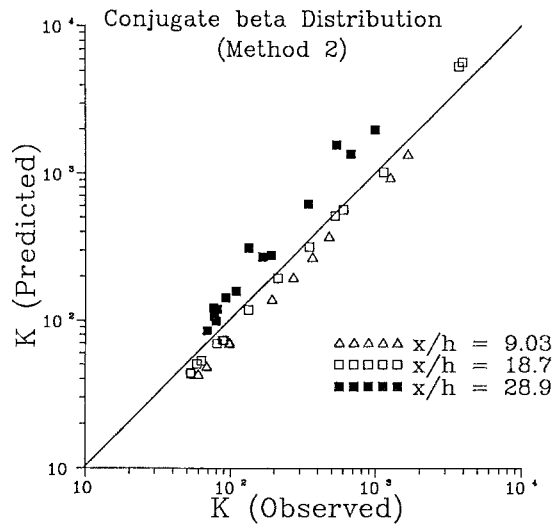

Fig. 18. Scatterplot of the observed total kurtosis versus the predicted total kurtosis for the conjugate beta distribution in which the parameters are estimated using the method of moments based on the conditional fluctuation intensity and skewness (Method 2). The data points were obtained at source height for various points in the cross-stream cross-section of the continuous plume at three downstream locations.

2) for calculating the model parameters, α and β, based on i_p^2 and S_p results in two scale-factor invariant (shape) parameters that can be obtained without requiring calibrated concentration data (either absolutely or relatively to one another). This is an important advantage for the analysis of concentration fluctuation data, especially in experimental systems where it is difficult to calibrate data accurately. The resulting model can be used to predict all scale-independent statistical quantities for describing concentration fluctuations (e.g., kurtosis (cf. Figure 18) and normalized concentration quantiles (cf. Figure 17)). However, if absolute statistical quantities are required for concentration fluctuations, the information in the mean concentration, $\overline{\chi_p}$, needs to be incorporated into the conjugate beta model. This could be achieved easily by introducing a scale parameter, σ, in the conjugate beta distribution (cf. Equation (A35)):

$$p(\chi) = \frac{\sigma}{B(\alpha, \beta)} \frac{(\sigma\chi)^{\alpha-1}}{(1+\sigma\chi)^{\alpha+\beta}}. \tag{12}$$

The scale-dependent information in the concentration fluctuations can be incorporated by choosing the scale parameter, σ, to match the mean concentration, $\overline{\chi_p}$, as follows:

$$\sigma = \frac{\alpha}{\overline{\chi_p}(\beta - 1)}. \tag{13}$$

Because the shape parameters, α and β, of the conjugate beta distribution exhibited in Equation (12) are scale-free, they can still be estimated using Equations (10) and (11).

6. Summary and Conclusions

It has been shown that the probability distribution function for the concentration data exhibits a highly asymmetrical form with a rather elongated exponential tail. The wide tail of the probability distribution, which implies the presence of large fluctuations within the plume, is markedly longer than that measured for dispersing scalars in the atmospheric boundary layer (e.g., Sawford, 1987; Dinar *et al.*, 1988; Mylne and Mason, 1991). The difference is probably due to the low mass diffusivity ($\mathrm{Sc} \approx 830$) of the saline tracer, and to the high resolution concentration sensors used in the present experiments. Both enhance the presence of sharp concentration gradients in the dispersing plume and lead to the observed wide-skirted pdf. The modal (i.e., most probable) value of in-plume concentration was only 10 to 20% of the mean concentration. The existence of this peak in the conditional pdf at a small concentration, coupled with the presence of the elongated tail (which is consistent with significant positive skewness and kurtosis of the in-plume concentration data) showed significant in-plume, small-scale intermittency within the instantaneous plume, adding to meandering intermittency produced by eddies much larger than the plume.

The shape and amplitude of the probability distributions for $\chi/\overline{\chi_p}$ did not significantly depend on the cross-stream position in the plume, in agreement with the rather weak dependence of the conditional concentration statistics on transverse position. However, mean shear near the ground surface increases mixing, altering the measured concentration pdfs in a vertical cross-section through the plume as i_p decreases and γ increases due to mixing.

Seven model distributions have been tested, namely, the lognormal, exponential, clipped normal, gamma, Weibull, conjugate beta and K-distributions. The commonly used clipped normal distribution was not supported by the data since the observed conditional fluctuation intensities, i_p, were greater than unity. With the exception of the conjugate beta distribution, all the candidate distributions generated curves in the (i_p^2, S_p) and (i_p^2, K_p) diagrams. The exponential distribution mapped into a single point on these diagrams. Since the normalized moments of the concentration data were found to cover a region (rather than falling on a curve) in the (i_p^2, S_p) and (i_p^2, K_p) diagrams, it was concluded that none of these six distributions adequately modeled the observed probability distribution of concentration at all the points within the dispersing plume. However, for points in the plume centerline taken at source height at various downstream fetches, it was found that the Weibull distribution provided the best match to the data, although this match was far from perfect, especially in the extreme upper tails. In particular, it has been shown that the Weibull distribution is capable of modelling adequately

the observed concentration pdf in the center to mid-extreme range of the data, but it overpredicts concentrations in the extreme upper tail for points in the meander-dominated stage of plume development and underpredicts the extreme concentration for points in the internal structure-dominated stage of plume development. In consequence, the Weibull distribution does not effectively represent all aspects of the statistical distribution of the concentration data and a more appropriate model distribution is required. Within the same context, the lognormal distribution has been shown to provide an upper bound for the total skewness and kurtosis, and the gamma distribution gave a lower bound for the predictions for these moments. Similarly, the quantiles of the gamma and lognormal pdfs have been shown to provide lower and upper bounds, respectively, for the data quantiles over the entire range of downstream fetches.

Almost all the normalized moments for concentration measured at a wide range of positions in the plume, lie on or above the line $S_p = 2i_p$ in the (i_p^2, S_p) plane that corresponds to the gamma distribution. It was shown that the conjugate beta distribution provides a versatile model for the probability distribution of concentration, because its parameters α and β allow it to cover the entire upper region of the (i_p^2, S_p) plane above the line $S_p = 2i_p$. This implies that the conjugate beta distribution is able to model adequately the statistical distribution of concentration data taken from a wide range of positions within the dispersing plume, without the necessity of changing its functional form (viz., only the two shape parameters that characterize the distribution need to change with the functional form of the distribution maintained). In the limit of $\beta \to \infty$ (α finite), the conjugate beta distribution asymptotically approaches the gamma distribution. Furthermore, since both parameters of the conjugate beta distribution appear in the expressions for the higher-order normalized moments (i.e., fluctuation intensity, skewness, kurtosis, etc.), this model permits a flexibility in the specification of model parameters to match some of the higher-order moments of the data.

The conjugate beta distribution for which the parameters are estimated using a method of moments based on i_p^2 and S_p (i.e., Method 2), provides an adequate model for the concentration probability distribution in the sense that the high concentrations in the plume are only slightly overestimated in the internal-structure dominated stage of plume development or underestimated in the meander-dominated stage of plume development. Finally, it should be noted that if interest is restricted to only peak concentrations for the prediction of risk of exposure, then the application of concepts from extreme-value statistics or recurrence statistics may lead to more appropriate models for the very high concentrations (Kristensen *et al.*, 1989).

Appendix A. Properties of Candidate Model Distributions

The relevant properties of seven model distributions considered in this paper are summarized. Since we want a distribution model to easily incorporate the various

higher-order moments of the concentration data, the first four moments of the model distributions are shown. Given a model pdf, $p(\chi)$, the evaluation of the mean, $\overline{\chi_p}$, relative fluctuation intensity, i_p^2, skewness, S_p, and kurtosis, K_p, involved calculating the k-th moment about the origin as

$$\mu_k' = \int_0^\infty \chi^k p(\chi)\, d\chi\,, \tag{A1}$$

exploiting algebraic relationships to convert these moments to moments about the mean (see, Spiegel, 1975), and then applying the appropriate definitions to the resulting central moments to construct the required normalized moments.

A.1. Exponential distribution

The exponential distribution has a pdf of the form

$$p(\chi) = \frac{1}{\delta}\exp\left(-\frac{\chi}{\delta}\right), \tag{A2}$$

where δ is the scale parameter. The associated cdf assumes the form

$$F(\chi) = 1 - \exp\left(-\frac{\chi}{\delta}\right). \tag{A3}$$

The mean, $\overline{\chi_p}$, relative fluctuation intensity, i_p^2, skewness, S_p, and kurtosis, K_p, for the exponential distribution are $\overline{\chi_p} = \delta$, $i_p^2 = 1$, $S_p = 2$, and $K_p = 9$.

A.2. Lognormal distribution

The lognormal distribution has a pdf of the form

$$p(\chi) = \frac{1}{\sqrt{2\pi}\,\sigma\chi}\exp\left(-\frac{\ln^2(\chi/m)}{2\sigma^2}\right), \tag{A4}$$

where m is the median and σ is the logarithmic standard deviation. The associated cdf assumes the form

$$F(\chi) = \frac{1}{2} + \frac{1}{2}\,\mathrm{erf}\left[\frac{\ln(\chi/m)}{\sqrt{2}\sigma}\right], \tag{A5}$$

where $\mathrm{erf}(x)$ denotes the error function. The mean, $\overline{\chi_p}$, relative fluctuation intensity, i_p^2, skewness, S_p, and kurtosis, K_p, for the lognormal distribution are given as follows:

$$\overline{\chi_p} = mu^{1/2}\,, \tag{A6}$$

$$i_p^2 = u - 1\,, \tag{A7}$$

$$S_p = \frac{u^3 - 3u + 2}{(u-1)^{3/2}}, \tag{A8}$$

and

$$K_p = \frac{u^6 - 4u^3 + 6u - 3}{(u-1)^2}, \tag{A9}$$

where $u \equiv \exp(\sigma^2)$ is the geometric variance.

A.3. Clipped normal distribution

The clipped normal distribution has a pdf of the form

$$p(\chi) = \frac{1}{\sqrt{2\pi} I \sigma_c} \exp\left(-\frac{1}{2}\left(\frac{\chi - \mu_c}{\sigma_c}\right)^2 \right), \tag{A10}$$

where

$$I \equiv \frac{1}{2}\left(1 + \operatorname{erf}\left(\frac{\mu_c}{\sqrt{2}\sigma_c}\right)\right), \tag{A11}$$

and μ_c and σ_c are location and scale parameters, respectively. The associated cdf assumes the form

$$F(\chi) = \frac{1}{2I}\operatorname{erf}\left(\frac{\mu_c}{\sqrt{2}\sigma_c}\right) + \frac{1}{2I}\operatorname{erf}\left(\frac{\chi - \mu_c}{\sqrt{2}\sigma_c}\right). \tag{A12}$$

The mean, $\overline{\chi_p}$, relative fluctuation intensity, i_p^2, skewness S_p, and kurtosis, K_p, for the clipped normal distribution are given as follows:

$$\overline{\chi_p} = \mu_c + \frac{\sigma_c}{\sqrt{2\pi} I} \exp\left(-\frac{1}{2}\frac{\mu_c^2}{\sigma_c^2} \right), \tag{A13}$$

$$i_p^2 = \frac{\mu_c}{\overline{\chi_p}} + \frac{\sigma_c^2}{\overline{\chi_p}^2} - 1, \tag{A14}$$

$$S_p = \frac{(i_p^2 + 1)(\mu_c/\overline{\chi_p} - 3) + 2\sigma_c^2/\overline{\chi_p}^2 + 2}{i_p^3} \tag{A15}$$

and

$$K_p = \frac{(i_p^2 + 1)(3\sigma_c^2/\overline{\chi_p}^2 + \mu_c^2/\overline{\chi_p}^2 - 4\mu_c/\overline{\chi_p} + 6) + 2\mu_c\sigma_c^2/\overline{\chi_p}^3 - 8\sigma_c^2/\overline{\chi_p}^2 - 3}{i_p^4}. \tag{A16}$$

A.4. Gamma distribution

The gamma distribution has a pdf of the form

$$p(\chi) = \left(\frac{\chi}{\delta}\right)^{k-1} \frac{\exp(-\chi/\delta)}{\delta\Gamma(k)}, \tag{A17}$$

where $\Gamma(x)$ is the gamma function and δ and k are scale and shape parameters, respectively. The associated cdf assumes the form

$$F(\chi) = \frac{\Gamma(k; \chi/\delta)}{\Gamma(k)} \tag{A18}$$

where $\Gamma(\nu; x)$ denotes the incomplete gamma function. The mean, $\overline{\chi_p}$, relative fluctuation intensity, i_p^2, skewness, S_p, and kurtosis, K_p, for the gamma distribution are given as follows:

$$\overline{\chi_p} = \delta k, \tag{A19}$$

$$i_p^2 = 1/k, \tag{A20}$$

$$S_p = 2/k^{1/2}, \tag{A21}$$

and

$$K_p = 3 + 6/k. \tag{A22}$$

A.5. Weibull distribution

The Weibull distribution has a pdf of the form

$$p(\chi) = \frac{r}{\beta}\left(\frac{\chi}{\beta}\right)^{r-1} \exp(-(\chi/\beta)^r), \tag{A23}$$

where β and r are scale and shape parameters, respectively. The associated cdf assumes the form

$$F(\chi) = 1 - \exp\left[-\left(\frac{\chi}{\beta}\right)^r\right]. \tag{A24}$$

The mean, $\overline{\chi_p}$, relative fluctuation intensity, i_p^2, skewness, S_p, and kurtosis, K_p, for the Weibull distribution are given as follows:

$$\overline{\chi_p} = \beta\Gamma(1 + 1/r), \tag{A25}$$

$$i_p^2 = \frac{\Gamma(1 + 2/r) - \Gamma^2(1 + 1/r)}{\Gamma^2(1 + 1/r)}, \tag{A26}$$

$$S_p = \frac{\Gamma(1+3/r) - 3\Gamma(1+1/r)\,\Gamma(1+2/r) + 2\Gamma^3(1+1/r)}{[\Gamma(1+2/r) - \Gamma^2(1+1/r)]^{3/2}}, \tag{A27}$$

and

$$K_p = \frac{\Gamma(1+4/r) - 4\Gamma(1+1/r)\Gamma(1+3/r) + 6\Gamma^2(1+1/r)\Gamma(1+2/r) - 3\Gamma^4(1+1/r)}{[\Gamma(1+2/r) - \Gamma^2(1+1/r)]^2}. \tag{A28}$$

A.6. K-DISTRIBUTION

The K-distribution has a pdf of the form

$$p(\chi) = \frac{4h^{\nu+1}}{\Gamma(\nu)}\chi^{\nu}K_{\nu-1}(2h\chi), \tag{A29}$$

where $K_\mu(x)$ is a modified Bessel function of the second kind of order μ, and h and ν are scale and shape parameters, respectively. The associated cdf assumes the form

$$F(\chi) = 1 - \frac{2h^{\nu}}{\Gamma(\nu)}\chi^{\nu}K_{\nu}(2h\chi). \tag{A30}$$

The mean, $\overline{\chi_p}$, relative fluctuation intensity, i_p^2, skewness, S_p, and kurtosis, K_p, for the K-distribution are given as follows:

$$\overline{\chi_p} = \frac{\sqrt{\pi}}{2h}\frac{\Gamma(\nu+1/2)}{\Gamma(\nu)}, \tag{A31}$$

$$i_p^2 = \frac{4\nu}{\pi s^2} - 1, \tag{A32}$$

$$S_p = \frac{(\sqrt{\pi}s/2)(3/4 - 3\nu/2 + \pi s^2/2)}{[\nu - \pi s^2/4]^{3/2}} \tag{A33}$$

and

$$K_p = \frac{2\nu(\nu+1) - 3\pi s^2/4 - 3\pi^2 s^4/16}{\nu^2(1 - \pi s^2/(4\nu))^2}, \tag{A34}$$

where $s \equiv \Gamma(\nu+1/2)/\Gamma(\nu)$.

A.7. CONJUGATE BETA DISTRIBUTION

The conjugate beta distribution has a pdf of the form

$$p(\chi) = \frac{1}{B(\alpha,\beta)}\frac{\chi^{\alpha-1}}{(1+\chi)^{\alpha+\beta}}, \tag{A35}$$

where $B(\alpha, \beta) \equiv \Gamma(\alpha)\Gamma(\beta)/\Gamma(\alpha + \beta)$, is the complete beta function and α and β are shape parameters. The associated cdf assumes the form

$$F(\chi) = \frac{B(\alpha, \beta; \chi/(1 + \chi))}{B(\alpha, \beta)}, \tag{A36}$$

where $B(a, b; x)$ denotes the incomplete beta function. The mean, $\overline{\chi_p}$, relative fluctuation intensity, i_p^2, skewness, S_p, and kurtosis, K_p, for the conjugate beta distribution are given as follows:

$$\overline{\chi_p} = \frac{\alpha}{(\beta - 1)}, \tag{A37}$$

$$i_p^2 = \frac{(\alpha + \beta - 1)}{\alpha(\beta - 2)}, \tag{A38}$$

$$S_p = \frac{2}{i_p}\frac{(2\alpha + \beta - 1)}{\alpha(\beta - 3)}, \tag{A39}$$

and

$$K_p = \frac{3(\beta - 2)[\alpha^3(\beta + 5) + 2\alpha^2(\beta - 1)(\beta + 5) + \alpha(\beta - 1)^2(\beta + 7) + 2(\beta - 1)^3]}{\alpha(\alpha + 1)^2(\beta - 1)^2(\beta - 3)(\beta - 4)}. \tag{A40}$$

Appendix B. Properties of Clipped Normal Distribution

The relative fluctuation intensity, i_p^2, skewness, S_p, and kurtosis, K_p, for the clipped normal distribution depend on only two dimensionless groups, namely $\overline{\chi_p}/\mu_c$ and $\overline{\chi_p}/\sigma_c$ (cf. Equations (A14) to (A16)). These two groups are a function of only the ratio, ρ, of the location parameter, μ_c, to the scale parameter, σ_c, for the clipped normal distribution (viz., $\rho \equiv \mu_c/\sigma_c$). In particular,

$$\frac{\overline{\chi_p}}{\mu_c} \equiv f(\rho) = 1 + \frac{1}{\sqrt{2\pi}\rho I(\rho)} \exp\left(-\frac{1}{2}\rho^2\right) \tag{B1}$$

and

$$\frac{\overline{\chi_p}}{\sigma_c} \equiv \rho f(\rho) = \rho\left(1 + \frac{1}{\sqrt{2\pi}\rho I(\rho)} \exp\left(-\frac{1}{2}\rho^2\right)\right), \tag{B2}$$

where

$$I(\rho) \equiv \frac{1}{2}(1 + \operatorname{erf}(\rho/\sqrt{2})). \tag{B3}$$

Consequently, it can be concluded that i_p^2, S_p, and K_p can be parametrized by the

parameter, ρ. As ρ varies from $-\infty$ to ∞, the clipped normal distribution traces out a curve in the $(i_p^2, S_p)((i_p^2, K_p))$ plane. Now, it is straightforward to show that $\lim_{\rho \to -\infty} i_p^2 = 1$ (cf. Equations (A14), (B1), (B2), and (B3)), $\lim_{\rho \to 0 \pm} i_p^2 = (\pi - 2)/2$, and $\lim_{\rho \to \infty} i_p^2 = 0$. However, $\mathrm{d}i_p^2/\mathrm{d}\rho \leq 0$ so i_p^2 is a monotonic non-increasing function of ρ on $(-\infty, \infty)$. Because i_p^2 is a monotonic non-increasing function on $\rho \in (-\infty, \infty)$ and $i_p^2 \to 1$ $(I \to 0)$ as $\rho \to -\infty$, this implies that $i_p^2 \leq 1$. Hence, in the limit $I \to 0$ (zero intermittency for the clipped normal distribution), $i_p^2 \to 1$ and the clipped normal distribution asymptotically approaches the exponential distribution.

References

Antonopoulos-Domis, M.: 1981, 'Large-Eddy Simulation of a Passive Scalar in Isotropic Turbulence', *J. Fluid Mech.* **104**, 55–79.

Bara, B. M., Wilson, D. J., and Zelt, B. W.: 1992, 'Concentration Fluctuation Profiles from a Water Channel Simulation of a Ground-Level Release', *Atmos. Environ.* **26A**, 1053–1062.

Chatwin, P. C. and Sullivan, P. J.: 1979, 'The Relative Diffusion of a Cloud of Passive Contaminant in Incompressible Turbulent Flow', *J. Fluid Mech.* **91**, 337–355.

Chatwin, P. C. and Sullivan, P. J.: 1987, 'The Probability Density Function for Contaminant Concentrations in Some Self-Similar Turbulent Flows', in *Proc. 2nd Intl Symp. on Transport Phenomena in Turbulent Flows*, Tokyo, pp. 215–226.

Csanady, G. T.: 1973, *Turbulent Diffusion in the Environment*, D. Reidel Publishing Company, Dordrecht, 248pp.

Deardorff, J. W. and Willis, G. E.: 1984, 'Ground-level Concentration Fluctuations From a Buoyant and Non-buoyant Source Within a Laboratory Convective Mixed Layer', *Atmos. Environ.* **18**, 1297–1309.

Dinar, N., Kaplan, H., and Kleiman, M.: 1988, 'Characterization of Concentration Fluctuations of a Surface Plume in a Neutral Boundary Layer', *Boundary-Layer Meteorol.* **45**, 157–175.

Durbin, P. A.: 1980, 'A Stochastic Model of Two Particle Dispersion and Concentration Fluctuations in Homogeneous Turbulence', *J. Fluid Mech.* **100**, 279–302.

Effelsberg, E. and Peters, N.: 1983, 'A Composite Model for the Conserved Scalar PDF', *Combust. Flame* **50**, 351–360.

Fackrell, J. E. and Robins, A. G.: 1982, 'Concentration Fluctuations and Fluxes in Plumes from Point Sources in a Turbulent Boundary Layer', *J. Fluid Mech.* **117**, 1–26.

Hanna, S. R.: 1984, 'The Exponential Probability Density Function and Concentration Fluctuations in Smoke Plumes', *Boundary-Layer Meteorol.* **29**, 361–375.

Hanna, S. R. and Insley, E. M.: 1989, 'Time Series Analysis of Concentration and Wind Fluctuations', *Boundary-Layer Meteorol.* **47**, 131–147.

Jones, C. D.: 1983, 'On the Structure of Instantaneous Plumes in the Atmosphere', *J. Haz. Mat.* **7**, 87–112.

Kaplan, H. and Dinar, N.: 1988, 'A Stochastic Model for Dispersion and Concentration Distribution in Homogeneous Turbulence', *J. Fluid Mech.* **190**, 121–140.

Kristensen, L., Weil, J. C., and Wyngaard, J. C.: 1989, 'Recurrence of High Concentration Values in a Diffusing, Fluctuating Scalar Field', *Boundary-Layer Meteorol.* **47**, 263–276.

Lewellen, W. S. and Sykes, R. I.: 1986, 'Analysis of Concentration Fluctuations from LIDAR Observations of Atmospheric Plumes', *J. Clim. and Appl. Meteorol.* **25**, 1145–1154.

Mylne, K. R. and Mason, P. J.: 1991, 'Concentration Fluctuation Measurements in a Dispersing Plume at a Range of up to 1000 m', *Q. J. R. Meteorol. Soc.* **117**, 177–206.

Sawford, B. L.: 1985, 'Lagrangian Statistical Simulation of Concentration Mean and Fluctuation Fields', *J. Climate Appl. Met.* **24**, 1152–1166.

Sawford, B. L.: 1987, 'Conditional Concentration Statistics for Surface Plumes in the Atmospheric Boundary Layer', *Boundary-Layer Meteorol.* **38**, 209–223.

Sawford, B. L., Frost, C. C., and Allan, T. C.: 1985, 'Atmospheric Boundary-Layer Measurements of Concentration Statistics from Isolated and Multiple Sources', *Boundary-Layer Meteorol.* **31**, 249–268.

Spanier, J. and Oldham, K. B.: 1987, *An Atlas of Functions*, Hemisphere Publishing Corporation, New York.

Spiegel, M. R.: 1975, *Probability and Statistics*, McGraw-Hill Book Company, New York.

Stapountzis, H., Sawford, B. L., Hunt, J. C. R., and Britter, R. E.: 1986, 'Structure of the Temperature Field Downwind of a Line Source in Grid Turbulence', *J. Fluid Mech.* **165**, 401–424.

Sykes, R. I., Lewellen, W. S., and Parker, S. F.: 1984, 'A Turbulent-Transport Model for Concentration Fluctuations and Fluxes', *J. Fluid Mech.* **139**, 193–218.

Thomson, D. J.: 1990. 'A Stochastic Model for the Motion of Particle Pairs in Isotropic High-Reynolds-Number Turbulence, and its Application to the Problem of Concentration Variance', *J. Fluid Mech.* **210**, 113–153.

Warhaft, Z.: 1981, 'The Interference of Thermal Fields from Line Sources in Grid Turbulence', *J. Fluid Mech.* **144**, 363–387.

Wilson, D. J.: 1991, 'Accounting for Peak Concentrations in Atmospheric Dispersion for Worst Case Hazard Assessments', *Proceedings AIChE/CCPS Conference on Modeling and Mitigating the Consequences of Accidental Release*, New Orleans, Louisiana.

Wilson, D. J., Robins, A. G., and Fackrell, J. E.: 1985, 'Intermittency and Conditionally-Averaged Concentration Fluctuation Statistics in Plumes', *Atmos. Environ.* **19**, 1053–1064.

Wilson, D. J. and Simms, B. W.: 1985, 'Exposure Time Effects on Concentration Fluctuations in Plumes', Report No. 47, Department of Mechanical Engineering, University of Alberta, Edmonton, Canada, 162 pp.

Wilson, D. J., Zelt, B. W., and Pittman, W. E.: 1991, 'Statistics of Turbulent Fluctuation of Scalars in a Water Channel', Technical Report for Defence Research Establishment Suffield (DRES-CR-31–91), Department of Mechanical Engineering, University of Alberta, Edmonton, Alberta, Canada, 60 pp.

Zelt, B. W., Wilson, D. J., and Bara, B.: 1987, 'Correcting Turbulent Concentration Measurements for Detector Spatial Resolution', *Proceedings 11th Canadian Congress of Applied Mechanics*, Edmonton, Alberta.